

An observer’s view of simulated galaxies: disc-to-total ratios, bars, and (pseudo-)bulges

Cecilia Scannapieco^{1,2}, Dimitri A. Gadotti^{2,3}, Patrik Jonsson⁴ and Simon D.M. White²

¹ *Astrophysical Institute Potsdam, An der Sternwarte 16, D-14482, Potsdam, Germany*

² *Max-Planck Institute for Astrophysics, Karl-Schwarzschild Str. 1, D-85748, Garching, Germany*

³ *European Southern Observatory, Casilla 19001, Santiago 19, Chile*

⁴ *Institute for Theory and Computation, Harvard-Smithsonian Center for Astrophysics, 60 Garden St., MS-51, Cambridge, MA 02138, USA*

22 October 2021

ABSTRACT

We use cosmological hydrodynamical simulations of the formation of Milky Way-mass galaxies to study the relative importance of the main stellar components, i.e., discs, bulges, and bars, at redshift zero. The main aim of this work is to understand if estimates of the structural parameters of these components determined from kinematics (as is usually done in simulations) agree well with those obtained using a photometric bulge/disc/bar decomposition (as done in observations). To perform such a comparison, we have produced synthetic observations of the simulation outputs with the Monte-Carlo radiative transfer code SUNRISE and used the BUDDA code to make 2D photometric decompositions of the resulting images (in the i and g bands). We find that the kinematic disc-to-total ratio (D/T) estimates are systematically and significantly lower than the photometric ones. While the maximum D/T ratios obtained with the former method are of the order of 0.2, they are typically > 0.4 , and can be as high as 0.7, according to the latter. The photometric decomposition shows that many of the simulated galaxies have bars, with Bar/T ratios in the range 0.2 – 0.4, and that bulges have in all cases low Sérsic indices, resembling observed pseudo-bulges instead of classical ones. Simulated discs, bulges and bars generally have similar $g - i$ colours, which are in the blue tail of the distribution of observed colours. This is not due to the presence of young stars, but rather to low metallicities and poor gas content in the simulated galaxies, which makes dust extinction low. Photometric decompositions thus match the component ratios usually quoted for spiral galaxies better than kinematic decompositions, but the shift is insufficient to make the simulations consistent with observed late-type systems.

Key words: galaxies: bulges – galaxies: formation – galaxies: fundamental parameters – galaxies: photometry – galaxies: structure – methods: numerical

1 INTRODUCTION

In the local universe, a significant fraction of the stellar mass is observed to be in discs (~ 60 per cent, Driver et al. 2007; Weinzirl et al. 2009 – see also Gadotti 2009). This is difficult to reconcile with simulations of galaxy formation in a Λ CDM universe, where hierarchical assembly tends to produce systems with a large fraction of their stellar mass in a bulge. In recent years, the inclusion of efficient treatments of supernova (SN) feedback, together with improved numerical resolution, have produced simulated disc galaxies more similar to real spirals (e.g. Brook et al. 2004; Governato et al. 2004; Scannapieco et al. 2008, 2009 and references therein), although although in most cases these are still dominated by

old, centrally concentrated spheroids. A limitation of these studies is the fact that comparison between simulations and observations is often rather crude, and the methods applied to derive structural parameters of simulated and observed galaxies are often very different. As a consequence, the results are not directly comparable, and it is hard to decide how close or how far from reality the simulated galaxies are. This is a serious problem since, in order to improve galaxy formation models, we need to know where we fail. Some recent studies have tackled this problem by analysing the simulated data to obtain ‘observables’ more directly comparable to observational results (e.g. Governato et al. 2009; Governato et al. 2010).

The main goal of this Letter is to perform a meaningful comparison between observations and simulations. To this end, we use a method we refer to as *photometric decomposition*, which consists of first producing synthetic images of simulated galaxies, and then performing 2D bulge/disc/bar decompositions to obtain their structural parameters and colours. In this way, we are able to mimic real observations and to directly compare, e.g., the derived scale-lengths, Sérsic indices, disc-to-total ratios, and colours with observational results. The simulations we use are those studied in Scannapieco et al. (2009, hereafter S09), which are cosmological hydrodynamical simulations of the formation of Milky Way-mass galaxies in a Λ CDM universe. Using a *kinematic* decomposition of the stars in the simulated galaxies, S09 found that 4/8 systems have significant disc components in rotational support, but the maximum disc-to-total (stellar mass) ratios they obtained is of the order of 0.2.

Here we analyse these simulations using the photometric decomposition technique which Gadotti (2009) applied to real galaxies to obtain structural parameters for discs, bars, classical bulges and pseudo-bulges. Gadotti's sample is particularly useful for a comparison, since it comprises galaxies with masses similar to that of the Milky Way (as in the simulations).

This Letter is organized as follows. In Section 2 we briefly describe the main characteristics of the simulations used in this study, as well as the methods to perform the kinematic and photometric decompositions. In Section 3 we show and discuss the outcome of the different techniques employed and compare results from photometric decompositions in simulated and real galaxies. Section 4 summarizes our results and conclusions.

2 METHODOLOGY

2.1 Simulation setup

For this study, we use the redshift $z = 0$ outputs of the simulations presented in S09, which correspond to eight galaxies with $z = 0$ masses similar to the Milky Way, assembled in the context of a Λ CDM cosmogony ($\Omega_\Lambda = 0.75$, $\Omega_m = 0.25$, $\sigma_8 = 0.9$ and $H_0 = 73 \text{ km s}^{-1} \text{ Mpc}^{-1}$). The initial conditions (ICs) are based on those generated for the Aquarius Project (Springel & et al. 2008) of the Virgo Consortium. To these dark-matter only ICs, we added baryons assuming $\Omega_b = 0.04$. Target haloes were selected to satisfy a mild isolation criterion at $z = 0$ (no neighbour exceeding half of their mass within 1.4 Mpc). All simulations have similar mass resolution, with dark matter and gas particle masses of the order of 2×10^6 and $3 \times 10^5 M_\odot$, respectively (see table 1 of S09 for details). We have used the same gravitational softening for dark matter, gas and star particles, which varies in the range 0.7 – 1.4 kpc for the different simulations. The halos have final masses in the range $7 - 16 \times 10^{11} M_\odot$, span a wide range in spin parameters (between 0.008 and 0.049), and have different merger and accretion histories. As a result, the galaxies present a variety of $z = 0$ morphologies (section 3 in S09).

The simulations have been run with the Tree-PM smoothed particle hydrodynamics (SPH) code GADGET-3 (Springel & et al. 2008), with the additional implementation of star formation and feedback as described in

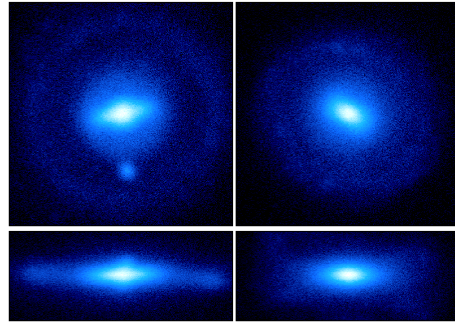


Figure 1. Face-on and edge-on SDSS *i*-band surface brightness images for Aq-C-5 (left-hand panels) and Aq-G-5 (right-hand panels), at $z = 0$. The images are 50 kpc across, and the edge-on images have a vertical depth of 20 kpc.

Scannapieco et al. (2005, 2006). Our model includes stochastic star formation, metal-dependent cooling, chemical enrichment and feedback from Type II and Type Ia SNe, with a multi-phase model for the gas component which avoids excessive cooling found in standard formulations of SPH, and allows winds to be generated naturally without additional *ad hoc* assumptions. We note that our implementation of star formation and feedback is different from that of Springel & Hernquist (2003), although we do use their treatment of UV background. More details on the simulation code, ICs and input parameters can be found in S09.

The *i*-band total magnitude of the simulated galaxies is in the range from -21 to -22 , which is similar to that of galaxies with stellar mass similar to that of the Milky Way, in the SDSS database (Kauffmann et al. 2003). Analogous results were found in the simulations by Governato et al. (2004) and Abadi et al. (2003a).

2.2 Photometric and kinematic decompositions

The *photometric* decomposition (PD) is done in two steps. First, we use the Monte-Carlo radiative-transfer code SUNRISE (Jonsson 2006; Jonsson et al. 2010) to generate face-on, synthetic images of the simulated galaxies in the *g* and *i* SDSS bands (examples of images are shown in Fig. 1). SUNRISE calculates the appearance of the simulated galaxy, from far-ultraviolet to submillimeter wavelengths, by tracing emitted radiation from the stellar particles through the dusty ISM of the galaxy, assuming that the density of dust grains traces the density of metals in the gas phase. The emission from dust grains is calculated for every location in the galaxy based on the intensity of radiation heating the dust grains, and is iterated to equilibrium. The final output is the spatially resolved emerging radiation from the simulated galaxy from a number of viewing angles, which can be directly compared to real observations. For more details about the radiation transfer calculation, the reader is referred to the above references.

To mimic the effects of a real observation, the SUNRISE images were convolved with a circular Gaussian function with FWHM of 1.5 pix, which corresponds to about 375 pc, or 0.75 arcsec, for a galaxy at a redshift of 0.03 and a plate scale of 0.5 arcsec per pix. With the same goal, we have multiplied these images by a factor such that their cen-

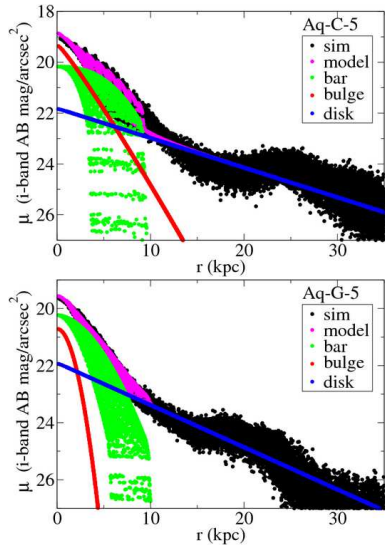


Figure 2. Results of the image decomposition (SDSS i band) for Aq-C-5 (upper panel) and Aq-G-5 (lower panel): surface brightness profiles of the simulated galaxies and the contribution of the different model components, as indicated. Each point corresponds to a single pixel (see Gadotti 2008 for details).

tral pixels have generally several thousand ADU, and also added a background pedestal of 200 ADU. As a second step, we perform a 2D bulge/disc/bar decomposition of the images using the BUDDA code (Gadotti 2008), and estimate the disc, bulge, and bar-to-total ratios, as well as the disc scale-length, bulge effective radius, and bulge Sérsic index. By combining results from the g and i bands, we also obtain the integrated $g - i$ colours of all components. The inclusion of bars is important since, as shown in e.g. Gadotti (2008), neglecting them (when present) in the modelling of galaxies can lead to large uncertainties in the estimation of bulge parameters, and a systematic overestimation of the bulge-to-total (B/T) ratio. In Table 1, we show the results of the PD, and in Fig. 2 we show the decomposition results for the two galaxies shown in Fig. 1. There are two cases, Aq-F-5 and Aq-H-5, for which a reliable decomposition was not possible, as these systems present unusual structural components. If these were real observations, these two galaxies would probably be excluded from the discussion. For completeness, we include these results, but they are always highlighted to remind the reader that they might not be reliable.

The *kinematic* decomposition (KD) assigns stars in the simulated galaxies to either a disc or a spheroidal component (see S09 for details). The decomposition is based on the distribution of $\epsilon \equiv j_z/j_{\text{circ}}$, where j_z is the angular momentum of each star perpendicular to the disc plane and j_{circ} is the angular momentum for a circular orbit at the same radius. We combine the distribution of ϵ with the radii of stars to define a disc component which does not suffer from contamination of spheroid stars in the inner regions (see Figs. 3 and 4 of S09). The spheroidal component is defined by stars that have not been tagged as disc stars and, as a result, it includes not only bulge and stellar halo stars, but also bar stars, when bars are present (visual inspection of the simulated galaxies indicates the presence of clear bars in about half the simulated galaxies). Once disc and spheroid stars

are identified, we estimate the (mass-weighted) disc-to-total (D/T^k , shown in Table 1) and spheroid-to-total ($1-D/T^k$) ratios, and the half-mass radii for both components. In the case of the disc, to be able to meaningfully compare the spatial scale with that obtained with the PD, we convert the half-mass radii into disc scale lengths, assuming an exponential surface mass density profile. The relation is such that the half-mass radius is 1.68 times the *scale-length*. Although, in some cases, the simulated disc profiles are not purely exponential, in particular because of the presence of outer rings, the assumption of an exponential profile is not expected to introduce errors, since the PD anyway assumes exponential profiles and, moreover, outer rings are also present in real galaxies.

3 RESULTS

3.1 Disc, bulge and bar to total ratios

The main result of this study is that the disc-to-total (D/T) ratios obtained from the kinematic and photometric decompositions differ significantly (Table 1 and Fig. 3). In most cases, the photometric D/T estimates are significantly higher than the kinematic ones. According to the KD, galaxies with significant disc components typically have $D/T \sim 0.2$ while the PD yields estimates of $0.4 - 0.7$. Moreover, for those galaxies with kinematically not very massive discs ($D/T \lesssim 0.09$), the photometric estimates can be as high as ~ 0.4 .

Although the KD estimates concern mass, while those from PD concern luminosity, this does not explain in this case such a discrepancy. As we will discuss further below, the mean stellar ages of the spheroid and disc components in the simulations are similar *and* they are both sufficiently old, meaning that differences in mass-to-light ratio between the different components are small. In fact, we find no significant difference when luminosity-weighted estimates (in the SDSS i band), calculated using the ages and metallicities of stars as inputs for the Bruzual & Charlot (2003) population synthesis models (for a Salpeter initial mass function as assumed in the simulations), are used (cf. open symbols in Fig. 3). Note that, in situations where disc and bulges have very different ages, this effect might however become important (Abadi et al. 2003b). These results clearly indicate the importance of comparing simulations with observations in an appropriate manner. According to our results, estimates for D/T ratios obtained from a kinematic decomposition can be much lower than those obtained from photometry by observational methods.

A possible source of the discrepancy between the D/T ratios obtained with the photometric and kinematic methods is that the former approach assumes an exponential profile for the discs, extending to the very centre. On the contrary, in the KD, disc stars are not present in the inner 2 kpc (see figure 4 in S09), since these central regions are purely dominated by velocity dispersion. In fact, the contribution of the inner 2 kpc to the total mass/luminosity for an exponential profile varies between 15 and 29 per cent, for $r_d = 6$ and 14 kpc (the range of scale lengths we find for our simulations). In other words, if we were to take kinematically identified disc particles and to fit an exponential

Table 1. Results from the kinematic and photometric decompositions of the eight simulated galaxies.

Galaxy (1)	D/T ^k (2)	D/T ^P (3)	B/T ^P (4)	Bar/T ^P (5)	$(g-i)_d$ (6)	$(g-i)_b$ (7)	$(g-i)_{bar}$ (8)	r_d^k (9)	r_d^P (10)	r_s^k (11)	r_{eff}^P (12)	n (13)
Aq-A-5	0.06	0.32	0.45	0.23	0.27	0.51	0.79	12.7	12.8	2.9	2.8	1.09
Aq-B-5	0.09	0.42	0.58	-	0.43	0.55	-	14.4	15.7	3.9	2.6	0.97
Aq-C-5	0.21	0.49	0.28	0.23	0.51	0.43	0.78	7.3	10.7	4.0	3.7	0.91
Aq-D-5	0.20	0.68	0.32	-	0.46	0.65	-	6.6	7.6	4.0	2.5	0.64
Aq-E-5	0.14	0.40	0.17	0.43	0.49	0.62	0.51	7.7	6.9	3.2	2.8	0.28
Aq-F-5	-	(0.44)	(0.56)	-	(1.02)	(0.59)	(0.51)	-	(13.4)	6.1	(4.3)	(1.02)
Aq-G-5	0.23	0.60	0.06	0.34	0.39	0.06	0.69	6.5	8.4	3.2	1.7	0.50
Aq-H-5	0.04	(0.05)	(0.95)	-	(1.34)	(-1.12)	(0.69)	6.3	(5.7)	4.2	(6.1)	(1.34)

Column (1) gives the designation of the simulated galaxy. Column (2) gives the disc-to-total estimated from the KD. Columns (3)-(5) show the disc, bulge and bar-to-total ratios obtained using the (SDSS i -band) photometric decomposition. Columns (6)-(8) give the $(g-i)$ colours of the disc, bulge and bar components, respectively. We give in columns (9) and (10) the disc scale-lengths (in kpc) obtained with the kinematic and photometric (i -band) decompositions, respectively. The kinematic half-mass radii for the spheroidal component and photometric (i -band) bulge effective radii are shown in columns (11) and (12) (both in kpc), and column (13) gives the photometric (i -band) bulge Sérsic index (n). Results for Aq-F-5 and Aq-H-5 obtained from the PD are given in parenthesis to remind the reader that these might not be reliable.

profile, we would get higher kinematic D/T estimates. We note, however, that this effect alone can not fully account for the differences in the D/T ratios between the two methods.

The differences in the D/T ratios can not be attributed to the particular band used in the analysis either. In fact, we have performed the PD for the g -band as well, and the results are similar to those obtained for the i -band. In particular, the B/T ratios and Sérsic indices change by less than 10 per cent (with the exception of Aq-G-5 where the g -band estimate is 45 per cent higher than the i -band one), and no systematics are detected. As for the D/T ratios, they are systematically ~ 5 per cent larger in the g -band (except for Aq-A-5, with a 20 per cent change). On the contrary, the Bar/T ratios are typically 20 per cent lower in the g -band. These changes are somewhat expected, considering that the youngest stars are in the discs, and bars are usually populated by old stars. It should also be noted that dust effects are negligible in the simulated images, due to their low metal and gas content. In fact, the typical face-on optical depth at the V band in the simulated galaxies is $\tau_V \approx 0.05 - 0.1$, which does not produce noticeable effects in bulge/disc decompositions (see Gadotti et al. 2010).

Another source of discrepancy between the D/T ratios obtained with the two methods is that a significant fraction (~ 40 per cent) of the stars outside the inner regions ($r > 5$ kpc) does not have disc-like kinematics; consequently they are not counted as disc particles in the KD, but they do contribute to the disc in the PD. The increase in the photometric D/T ratio due to this effect is, nevertheless, not expected to be very high, since the light from the disc region is always dominated by young stars on near-circular orbits.

Another result of the photometric analysis is the detection of bars, which, when present, can be quite prominent, with Bar/T between 0.23 and 0.43 (Table 1), values typical of observed strong bars (Gadotti 2008). This also means that, even for moderate D/T values, the bulges do not necessarily dominate over discs (Table 1). In fact, all galaxies with bars have D/T > B/T. One interesting finding is that Aq-G-5 has a quite low B/T: only 6 per cent of the stellar luminosity is associated to the bulge. In this galaxy, the disc

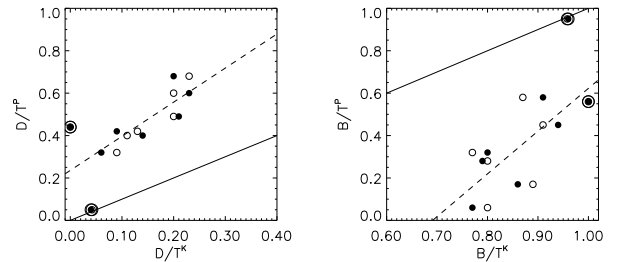


Figure 3. Photometric versus kinematic results for the D/T and B/T ratios. In the case of the KD, we include mass-weighted (filled symbols) and luminosity-weighted (open symbols) estimates. The solid lines depict the one-to-one correspondence, and the dashed lines a linear fit to the data, excluding Aq-F-5 and Aq-H-5 (encircled symbols) for which the results of the PD might not be reliable. The observed D/T in local late-type galaxies, with stellar masses similar to that of the Milky Way, ranges from about 0.7 to 1, while for B/T the corresponding value ranges from 0 to 0.2 (Gadotti 2009).

and bar contributions to the total luminosity are 60 and 34 per cent, respectively. We also find cases of bulge-dominated galaxies (the highest B/T we find are of the order of 0.6), such as Aq-A-5 and Aq-B-5 (as well as Aq-F-5 and Aq-H-5). Among these, some have bars and some do not.

3.2 $g-i$ Colours, spatial scales and Sérsic indices

The $g-i$ integrated colours of the different components (bulge, disc and bar) were obtained directly from the BUDDA models corresponding to the g and i band images. We find that, generally, the three components have similar $g-i$ colours, which differ typically by only 0.1–0.2 mag (Table 1). Furthermore, all components show $g-i$ colours which are in the blue tail of the corresponding distribution for real galaxies found in Gadotti (2009). The finding that all components have similar $g-i$ colours can be understood in terms of the following properties: (i) the mean ages of disc and spheroidal stars differ typically by only ~ 3 Gyr (typical ages for the

disc and spheroidal components are 7.5–9 and 11–12 Gyr, respectively – see table 2 of S09; with two two exceptions, Aq-A-5 and Aq-B-5, which have very young discs), (ii) the distributions of $[\text{Fe}/\text{H}]$ of bulge and disc stars peak at low values, about -0.5 and -1 , respectively, and differ by only a few tenths of a dex, the bulge stars generally having higher values of $\log [\text{Fe}/\text{H}]$, and (iii) the amount of leftover gas at $z = 0$ is small, and so is the amount of dust. As a result, the $g - i$ colours reflect those of a stellar population which is blue due to low metallicity. Overall, our results are consistent with these simulated galaxies being disc-dominated, late-type systems, with low $[\text{Fe}/\text{H}]$.

We have also compared the typical spatial sizes of discs, obtained with the two decompositions. As explained above, we have converted the half-mass radii of S09 into a corresponding scale-length assuming an exponential surface density profile. The two estimates [columns (9) and (10) of Table 1, respectively] agree well with the range observed in real (late-type) galaxies (between ~ 1 and ~ 8 kpc – see figure 18 in (Gadotti 2009)), although they are in the high-end tail. In real galaxies, the largest values for the disc scale-lengths are usually found in galaxies with low B/T.

In columns (11)-(13) of Table 1, we show the half-mass radii of the spheroidal components obtained with the KD, and the bulge effective radii and Sérsic indices from the PD, respectively. We discuss these results separately from those presented before, noting that they may be affected by numerical resolution as the bulge scale-lengths obtained with both decompositions are between 2 and 4 times the corresponding gravitational softening (except for Aq-G-5, where the bulge effective radius is of the order of the softening length). However, we do not find a correlation between the gravitational softening length and the bulge scale-lengths, so our results are not necessarily softening dominated. The PD estimates for the bulge effective radii and the KD estimates for the spheroidal half-mass radii are similar, and are significantly larger than the bulge effective radii observed in real galaxies, which are typically about 1 kpc (see table 3 in Gadotti 2009). As for the the Sérsic indices, we find that $n \lesssim 1$ in *all* cases (Table 1). In this aspect, these bulges resemble pseudo-bulges rather than classical ones (see, however, section 4.2 in Gadotti 2009). This result is intriguing since these galaxies have undergone mergers (although mainly minor ones), which are generally expected to produce classical bulges. The origin of bulges in these simulations and its relation to Sérsic indices will be investigated in detail in a separate work.

4 CONCLUSIONS

We have analysed the $z = 0$ outputs of eight cosmological, hydrodynamical simulations of the formation of Milky Way-mass galaxies, focusing on the study of the relative importance of the main stellar components, i.e., bulges, discs and bars. We have used two different analysis techniques: a kinematic decomposition of stars into disc and spheroidal components, widely used in simulation studies, and a photometric decomposition into bulge, disc and bar components, as applied to observations. Using both approaches, we estimated disc-to-total ratios and disc and bulge scale-lengths. The photometric decomposition also allowed us to compute

the $g - i$ colours of the different components, the bulge Sérsic index, and bulge- and bar-to-total ratios, and to compare them directly, and in a meaningful manner, to observational results obtained using the same techniques.

We found that the photometric and kinematic decompositions predict different D/T ratios; those obtained with the former method are systematically higher than those from the latter. The discrepancy cannot be attributed to the fact that contributions to the different components are mass-weighted for the KD and luminosity-weighted for the PD, and are not particular to the band used in the PD (similar results are obtained for the i and g bands). In part, the discrepancy can be explained considering that, in the KD, disc stars are not present within the inner ~ 2 kpc, while the PD assumes an exponential profile starting at the centre of the galaxy. This comparison is of relevance, since it indicates that the kinematic structure of real galaxies may not be correctly inferred from the D/T ratios provided by photometric analysis. When simulations are analysed in the same way as observations, their properties appear closer to those of real galaxies than when a KD is performed, although none of our simulations comes close to reproducing a late-type, fully disc-dominated galaxy.

According to the PD, half of the simulated galaxies have significant bar components. A consequence of this result is that, even in galaxies with relatively low D/T ratios, bulges do not necessarily dominate over discs. The presence of bars makes the comparison between the two methods even harder since, in the kinematic approach, bars are counted as part of the spheroidal component. Results of the PD also show that all components have similar $g - i$ colours, in the blue tail of the observed distribution. This is understood in terms of all components having low metallicity, relatively similar ages, and low gas/dust content at $z = 0$.

We find good agreement between the disc scale-lengths obtained with our two methods. In the case of the bulges, however, a conclusion is harder to make, since the bulge scale-lengths are typically a few times the size of the gravitational softening and thus may be affected by resolution, although there is no correlation between bulge size and assumed softening. We also find that Sérsic indices are in all cases near unity, making the simulated bulges more similar to observed pseudo-bulges rather than to classical ones.

The results of this work suggest that, in order to be meaningfully confronted with observations, results from simulations need to be analysed following observational techniques. On the other hand, simulations contain valuable information that can be used to better interpret observations, and they allow the physical processes contributing to shape a galaxy's morphology to be studied. We hope our work is a step towards encouraging the exchange of expertise between observers and simulators, since a lot of physical insight can be gained from such an exchange.

ACKNOWLEDGMENTS

We thank the referee for a thorough reading of this work and for helpful comments and suggestions. The authors acknowledge useful discussions with E. Athanassoula, P. Coelho, R. de Jong, P. Ocvirk and V. Springel.

REFERENCES

- Abadi M. G., Navarro J. F., Steinmetz M., Eke V. R., 2003a, *ApJ*, 591, 499
- Abadi M. G., Navarro J. F., Steinmetz M., Eke V. R., 2003b, *ApJ*, 597, 21
- Brook C. B., Kawata D., Gibson B. K., Freeman K. C., 2004, *ApJ*, 612, 894
- Bruzual G., Charlot S., 2003, *MNRAS*, 344, 1000
- Driver S. P., Allen P. D., Liske J., Graham A. W., 2007, *ApJl*, 657, L85
- Gadotti D. A. 2008, *MNRAS*, 384, 420
- Gadotti D. A. 2009, *MNRAS*, 393, 1531
- Gadotti D. A., Baes M., Falony S., 2010, *MNRAS*, p. 117
- Governato F., Brook C., Mayer L. et al., 2010, *Nature*, 463, 203
- Governato F., Brook C. B., Brooks A. M. et al., 2009, *MNRAS*, 398, 312
- Governato F., Mayer L., Wadsley J. et al., 2004, *ApJ*, 607, 688
- Jonsson P. 2006, *MNRAS*, 372, 2
- Jonsson P., Groves B. A., Cox T. J., 2010, *MNRAS*, 403, 17
- Kauffmann G., Heckman T. M., White S. D. M., et al., 2003, *MNRAS*, 341, 33
- Scannapieco C., Tissera P. B., White S. D. M., Springel V., 2005, *MNRAS*, 364, 552
- Scannapieco C., Tissera P. B., White S. D. M., Springel V., 2006, *MNRAS*, 371, 1125
- Scannapieco C., Tissera P. B., White S. D. M., Springel V., 2008, *MNRAS*, 389, 1137
- Scannapieco C., White S. D. M., Springel V., Tissera P. B., 2009, *MNRAS*, 396, 696 (S09)
- Springel V., et al., 2008, *MNRAS*, 391, 1685
- Springel V., Hernquist L., 2003, *MNRAS*, 339, 289
- Weinzirl T., Jogee S., Khochfar S., Burkert A., Kormendy J., 2009, *ApJ*, 696, 411